

Electron Microscopy Visualization of Vitronectin Adsorbed on $-\text{COOH}$ and $-\text{NH}_2$ Functionalized Surfaces: Distinctive Spatial Alignment and Regulated Cellular Responses

Wenjia Hou, Yi Liu, Botao Zhang, Xiaoyan He, and Hua Li*

Adsorption of proteins associating with their conformational changes plays crucial roles in regulating biomaterial–cell interactions and consequent tissue responses to implanted biomaterials. This study reports direct visualization of typical serum protein, vitronectin, one of the key adhesive proteins that participate in mediating cell behaviors, upon adsorption on typically designed surfaces. Carbon films with their surfaces being plasma grafted functional groups $-\text{COOH}$ and $-\text{NH}_2$ are used as the model substrata for this study. Negative-staining electron microscopy technique is employed for visualizing the adsorbed protein and 2D image classification is made and interpreted. Results show that adsorbed vitronectin tends to form multimer aggregate on the $-\text{COOH}$ -grafted surfaces, exposing extensively its cell-binding RGD (arginine-glycine-aspartic acid) motif for enhanced cell adhesion. The adsorbed vitronectin on the $-\text{NH}_2$ -grafted surface forms dimer aggregate with the binding sites being enwrapped. The $-\text{COOH}$ -grafting triggers enhanced expressions of *ITGA5*, *ITGAV*, *ITGB1*, and *ITGB3* of the adhered cells and this is likely attributed to the special spatial alignment of vitronectin upon adsorption. The conformational information of adsorbed vitronectin gained from the single particle electron microscopy analyses would shed light on design and construction of appropriate biomaterials surfaces for desired cellular behaviors.

1. Introduction

Appropriate response of tissue cells to biomaterials is one of the essential prerequisites for successful implantation after surgery. Many efforts have been devoted to understanding the dynamic interactions between cells and biomaterials.^[1] It is established that upon contact with body tissue, biomaterials are coated with a layer of serum proteins within milliseconds, which is

considered to be the most important factor deciding cell–biomaterial interactions.^[2] As one of the major cell adhesive proteins in serum-containing cell culture, vitronectin (Vn) is usually organized into distinct domains according to alternative functional properties, participating in blood coagulation, fibrinolysis, cell adhesion, and tissue remodeling.^[3] These biological activities of Vn are directly dependent on its conformation. Protein adsorption could trigger protein conformational changes in a controllable manner. The cell-binding motif RGD (arginine-glycine-aspartic acid), the principal ligand for the integrin family of adhesion receptors on Vn, has been reported to be cryptic in the native form of Vn in solution.^[4] Changes in conformation of adsorbed Vn may affect its RGD motif exposure,^[5] in turn regulating the biocompatibility of implanted surfaces. It is known that various surface characteristics, such as chemistry, wettability, charge, and stiffness, could lead to different conformations of Vn after adsorption.^[6] Challenges

yet remain as to how to characterize the structure of the protein upon adsorption, and the impact of its conformational characteristics on cellular behaviors needs to be elucidated.

Early efforts on identifying the structures of Vn adsorbed on typical hydrophobic and hydrophilic surfaces were made employing polarity-sensitive fluorophore acrylodan, and results evidenced that the domains surrounding the free sulfhydryl groups of Vn experienced different environments in solution from those on adsorbed surfaces.^[5] Analysis of the secondary structure of Vn using infrared spectroscopy and circular dichroism revealed a reduction in β -sheet structure upon adsorption on polystyrene or oxidized polystyrene.^[7] To date, a variety of techniques, for instance atomic force microscopy (AFM), X-ray photoelectron spectroscopy (XPS), time of flight secondary ion mass spectrometry, and quartz crystal microbalance, have been used to study the structure of adsorbed proteins.^[8] Most of the acquired structural information pertains to the secondary structure and orientation of adsorbed Vn. Direct visualization of Vn upon adsorption for clarifying its conformational changes is yet lacking. Reconstruction of classified 2D or even 3D structure of adsorbed Vn is essentially required for comprehensively understanding how cell–biomaterial interaction takes place and functions at molecular level.

Dr. W. J. Hou, Dr. Y. Liu, Dr. B. Zhang, Dr. X. He, Prof. H. Li
Key laboratory of Marine Materials and Related Technologies
Zhejiang Key Laboratory of Marine Materials and Protective Technologies
Ningbo Institute of Materials Technology
and Engineering
Chinese Academy of Sciences
Ningbo 315201, China
E-mail: lihua@nimte.ac.cn

Dr. W. J. Hou
College of Materials Science and Opto-Electronic Technology
University of Chinese Academy of Sciences
Beijing 100049, China

 The ORCID identification number(s) for the author(s) of this article can be found under <https://doi.org/10.1002/admi.201700958>.

DOI: 10.1002/admi.201700958

Small-angle X-ray measurement has been taken to generate a 3D model of human plasma Vn.^[9] The 51-residue N-terminal domain comprises binding sites for PAI-1,^[10] integrins,^[11] and uPAR.^[12] The first 44 amino acids in the N-terminal domain are named somatomedin B domain and their structure has been resolved by NMR.^[13] In addition, the central domain is composed of residues 131–323 and houses the binding sites for bacteria.^[14] The C-terminal domain of Vn, comprising residues 354–456, is thought to provide binding sites for heparin and complement factors.^[15] It was reported that the wide separation between N- and C-terminal domains of Vn frees up extensive room on the surface to form multimeric complex.^[15a] Most importantly, the RGD binding site of Vn lies between residues 45 and 47,^[13] which locates within a flexible region, next to the relatively unstructured linker sequence between N- and central-domains. Physicochemical characteristics of biomaterials at their surfaces may play crucial roles in deciding possible reorganization of the spatial conformation of Vn upon its adsorption, which in turn affects subsequent recruitment and adhesion of cells.

To elucidate the conformational changes of the serum protein after its adsorption on biomaterials surfaces, in this work, the adsorbed Vn molecules were examined by negative-staining electron microscopy (EM). Since protein conformation is largely correlated with surface charge,^[6b] –COOH- and –NH₂-functionalized carbon films were used as the typical surfaces for the adsorption testing. 2D image classification and interpretation revealed distinctive spatial alignment of Vn molecules adsorbed on the surfaces. Further clarification of enhanced exposure of cell-binding domain of Vn and changes in integrin gene expression of human osteoblast cells adhered on the functionalized surfaces would give insights into design and appropriate modification of biomaterials for desired cellular behaviors.

2. Results and Discussion

To characterize the plasma-grafted functional groups, XPS measurements were taken (Figure 1A). Chemistry of the carbon films coated on silicon wafer was analyzed through the

features of the C-1s peak. The peak at 284.6 eV is assigned to hydrocarbon (CH_x), and the peaks at 286.1 and 287.7 eV are likely attributed to C–O (alcohol or ether) and C=O (carbonyl), respectively. For the C-1s core spectrum of grafted acrylic acid, notably, the peak located at 288.3 eV refers to C(=O)O, suggesting successful grafting of –COOH groups on carbon films. For the film with plasma grafted allylamine, increase in nitrogen content on its surface is detected (Table 1). Examination of the C-1s core level shows a decrease in the relative intensity of C=O and C–O peaks, and the appearance of a peak at 285.3 eV is seen, which is assigned to C–N bonds, indicating presence of primary, secondary, tertiary, or quaternary amines. In addition, the grafting of the functional groups –COOH and –NH₂ is further evidenced by the altered wettability of the films (Figure 1B). Significantly decreased water contact angle is seen after the plasma grafting treatment, from 64.6° to 28.3° for the acrylic acid treated sample and from 64.6° to 43.4° for the allylamine treated sample. Plasma grafting is a widely used method to obtain monofunctional surfaces.^[16] Previous studies have demonstrated that terminal chemical groups could affect protein adsorption and cell behaviors including adhesion, migration, and differentiation.^[6b,d,17] In this case, XPS spectra and water contact angle measurements show that –COOH- and –NH₂-terminal groups were successfully grafted.

Protein adsorption is a slow protein denaturation process,^[18] and its conformation usually encounters changes upon adsorption.^[19] To visualize possible conformational changes of adsorbed Vn directly, single particle negative-staining EM technique was employed in this study. This technique has been used as a powerful tool for direct imaging of large macromolecules for reconstruction of their 3D structures. EM observation of Vn clearly suggests the fast adsorption of Vn on the –COOH- and –NH₂-treated surfaces (Figure 2A-1,A-2). Protein adsorption is usually codetermined by van der Waals and electrostatic interactions, and van der Waals interaction plays the predominant role at low surface charge density, while at high surface charge density, electrostatic interaction dominates.^[20] In the EM images, Vn adsorption on the untreated surface is rarely seen (data not shown), which could be attributed to the fact that the capillary force brought about by blotting is larger than van der Waals for adsorbed Vn. However, it is likely that

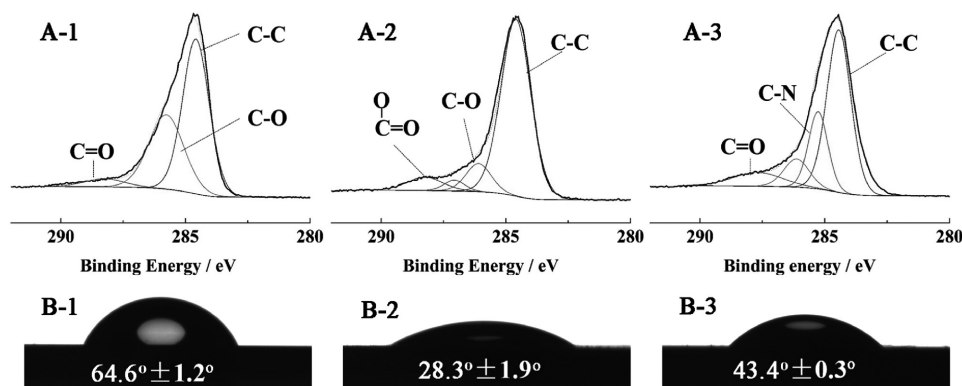


Figure 1. Characteristics of the plasma-grafted carbon films for the protein adsorption testing (1: the untreated sample, 2: the –COOH-grafted sample, 3: the –NH₂-grafted sample). A) XPS spectra of the samples (all the spectra were charge-corrected to the C–C 1s core level at 284.6 eV), and B) digital photos showing water contact angles of the samples.

Table 1. XPS analyses of the substrata grafted with the different terminal groups.

	C1s [wt%]	O1s [wt%]	N1s [wt%]
Untreated	66.96	33.03	–
Plasma-grafted acrylic acid	67.39	32.14	0.47
Plasma-grafted allylamine	61.29	36.27	2.45

electrostatic interaction decides the adsorption on the $-\text{COOH}$ - and the $-\text{NH}_2$ -modified surfaces. In addition, it is noted that there is no significant difference in amount of adsorbed Vn on the functionalized surfaces (Figure 2A-1,A-2). Surprisingly, however, the molecules exhibit distinctive morphologies on the two films. Further 2D classification reveals clearly aggregation of Vn in specific manners, which correlates with the surface features of the substrata (Figure 2B-1,B-2). The selected averaged images suggest distinctive agglomeration of Vn molecules on the functionalized surfaces. For the $-\text{COOH}$ -terminated film,

Vn opts to form multimer aggregate upon adsorption, showing a globular shape with an average diameter of ≈ 20 nm. This result is in good agreement with a previous report claiming that Vn adsorbed as globular aggregates with a size between 15 and 28 nm.^[21] By contrast, Vn forms dimer aggregate upon adsorption on the $-\text{NH}_2$ -grafted surface (Figure 2B-2). Our finding reveals the distinctive spatial alignment of Vn on the typically designed surfaces. Preliminary docking of the atomic N-terminal domain structure of Vn (1S4G, PDB databank)^[13] into the selected 2D classes (Figure 2C-1,C-2) further confirms the observations that upon adsorption on the $-\text{NH}_2$ -grafted surface, two monomers exactly stand side by side with one being curved with the dimension of ≈ 9 nm in length and ≈ 3 nm in width, and the other being much shorter (Figure 2C-2). For each aggregate formed on the $-\text{COOH}$ -grafted surfaces, “O” shaped conformation is seen, containing ≈ 9 monomers (Figure 2C-1). Previous small-angle scattering measurement revealed Vn to be peanut-shaped,^[9] and for comparison purpose, the proposed model is also shown here (Figure 2D). Our direct visualization reveals similar conformation of Vn (Figure 2C-2 vs Figure 2D).

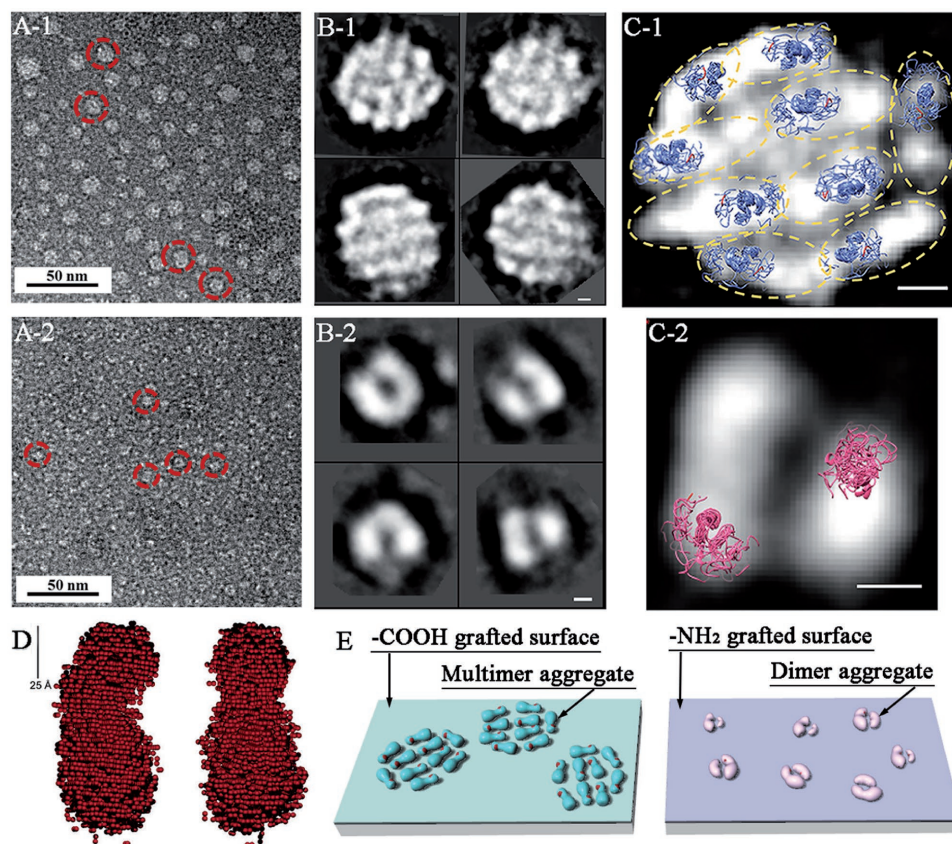


Figure 2. Negative-staining EM images and image analyses of Vn adsorbed on the surfaces of the samples. A) Representative raw EM images of the Vn molecules in uranyl acetate stain adsorbed on the $-\text{COOH}$ -grafted surface (A-1) and on the $-\text{NH}_2$ -grafted surface (A-2). B) Selected 2D averaged images of Vn molecule adsorbed on the $-\text{COOH}$ -grafted surface (B-1) and on the $-\text{NH}_2$ -grafted surface (B-2). C) Preliminary docking of the N-terminal NMR domain structure of Vn (1S4G, PDB databank, ref. [13]) into the selected 2D images showing spatial alignment of the molecules (C-1, C-2, the atomic structure in blue color represents the N-terminal domain of the molecule adsorbed on the $-\text{COOH}$ grafted surface, and the structure in pink color represents the N-terminal domain of the molecule adsorbed on the $-\text{NH}_2$ -functional surface). D) A previously proposed 3D structure model as determined by small-angle scattering measurement^[9] showing similar conformation of Vn. E) The proposed model illustrating the spatial alignment of Vn molecules upon their adsorption on the surfaces (the parts in blue and pink colors are the intact structure of Vn adsorbed on the $-\text{COOH}$ and $-\text{NH}_2$ modified films, and the cell binding domain is highlighted by red color). The scale bars in (B-1), (B-2), (C-1), and (C-2) are 2.5 nm.

Preliminary docking of the NMR N-terminal structure of Vn,^[13] the only available high-resolution domain structure of Vn, presumably identifies the spatial alignment of ≈ 9 monomers for forming the multimer aggregate on the $-\text{COOH}$ functionalized surface (Figure 2C-1). It is known that to gain sufficient information about the alignment, 3D structure of the aggregate is essentially required. However, due to the fact that Vn prefers to adsorb on the surface in a specific manner (for instance lying on the surface, Figure 2B-2,C-2), it is not possible to collect all views of the protein particles necessarily required for 3D reconstruction. Even though the resolution of the EM images is insufficient for clarifying the atomic structure of Vn, our attempt already provides helpful clues to understanding preferential adsorption of Vn. The alignment of the monomers is schematically depicted in Figure 2E. The structural evolution in terms of specific aggregation of Vn molecules after their adsorption on the surfaces should exert significant impact on following cellular behaviors.

Vn is a multidomain protein and has both positively charged and negatively charged regions. In the native state, the highly acidic residues in the amino terminus of Vn are believed to interact with the positively charged basic residues. This interaction could stabilize the entire Vn molecule in a relatively closed conformation, and forces the cell-binding domain into one location.^[22] When adsorption occurs, many ligand-binding domains within Vn molecule appear to be differentially exposed according to appropriate conformation of the adhesive protein. A heparin-binding domain at residues 341–379 contains a large number of positively charged amino acids, having high affinity to the negatively charged ($-\text{COOH}$ -terminated) surface.^[5] In addition, the central heparin binding region is one of the main factors for inducing multimerization of Vn.^[21] These could explain why Vn prefers to form multimer aggregates on the $-\text{COOH}$ -grafted surfaces rather than on the $-\text{NH}_2$ -treated surfaces.

To further reveal the conformational changes of Vn after the adsorption, the exposure extent of its cell-binding domain was examined by the ELISA test. It is known that the cell-binding site of Vn is composed of tripeptide sequence RGD motif, lying between residues 45 and 47, and interacts with integrins in osteoblast membrane. V58-1, a mono antibody that specifically reacts with an epitope of the residues 1–130 of human Vn, can be used as the primary antibody to assess the exposure state of the RGD motif on Vn. It is surprisingly found that the amount of the 2nd antibody, which indicates exposure state of cell-binding domains of all the molecules adsorbed on the surfaces, shows significantly different values (Figure 3). The 2nd antibody exhibits higher value for the molecules adsorbed on the $-\text{COOH}$ -grafted surface than on the $-\text{NH}_2$ -grafted surface (Figure 3), suggesting that adsorption of Vn does not necessarily mean favorite exposure of its RGD binding site for cell adhesion. The exposure ratio of the cell-binding site for each molecule could be determined by the ratio of the amount of 2nd antibody to the total amount of the adsorbed Vn. It is clear that the $-\text{NH}_2$ -functionalized surface holds the lowest exposure ratio of the cell-binding site for each molecule, whereas the $-\text{COOH}$ -grafted surface shows the highest exposure ratio. This phenomenon was also reported by other researchers.^[6c] Taking into account the EM conformations of the adsorbed Vn (Figure 2),

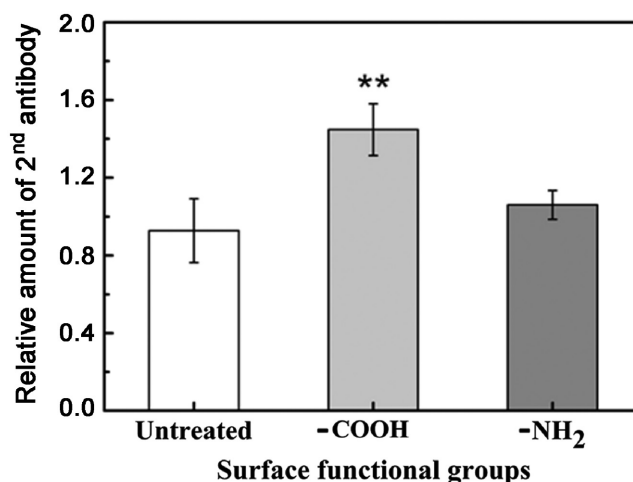


Figure 3. The relative amount of adsorbed Vn as estimated by ELISA test using V58-1 as the primary antibody. Error bars refer to standard deviation ($n = 5$), $**p < 0.01$ as compared with the control samples (analyzed by paired Student's *t*-test).

it is clear that Vn prefers to form multimer aggregates on the $-\text{COOH}$ -charged surface, exposing a large amount of cell-binding domains, whereas opts to form dimmer on the $-\text{NH}_2$ -modified surface with the binding sites being wrapped.

It has been demonstrated that cell-binding function of Vn is mainly mediated by its RGD motif, which is located next to the highly acidic and negatively charged region.^[18] This negatively charged polar is expected to be pushed away from the negatively charged surface, $-\text{COOH}$ -terminated surface in this case, through electrostatic repulsions, in turn resulting in enhanced exposure of the RGD motif. This speculation is evidenced by our results (Figure 3). In addition, the conformation of adsorbed protein might also be affected by surface roughness of substrate. AFM measurements show that R_q values of the untreated surface, the $-\text{COOH}$ -functionalized surface, and the $-\text{NH}_2$ -functionalized surface are 0.91, 0.89, and 1.26 nm, respectively. The minor differences imply that in this case, the roughness might not be one of the main factors affecting the adsorption behaviors of Vn. It could therefore be concluded that the conformation of adsorbed Vn is mainly dominated by surface charge of the substrata. To further confirm this, Vn was diluted in PBS and the same treatment was done as that diluted in Milli-Q water. Result shows that no matter on the $-\text{COOH}$ -functionalized surface or on the $-\text{NH}_2$ -functionalized surface, Vn forms multimeric aggregates with similar size (Figure S1, Supporting Information). In this case, it is considered that Vn has already undergone a multimerization in PBS because of the presence of anions in the electrolyte solution. Our results are consistent with other reported findings that Vn is more likely to form multimer or encounters self-association in PBS.^[5]

Further cell culturing reveals the impact of the conformational changes of adsorbed Vn on following cellular behaviors. After 4 h incubation, attachment and spreading of human osteoblast cells are clearly seen on the surfaces of the films with/without preadsorption of Vn (Figure 4). The cytoskeleton structure of the cells was examined using fluorescence microscopy. It is clear that the cells adhering on the Vn-preadsorbed samples

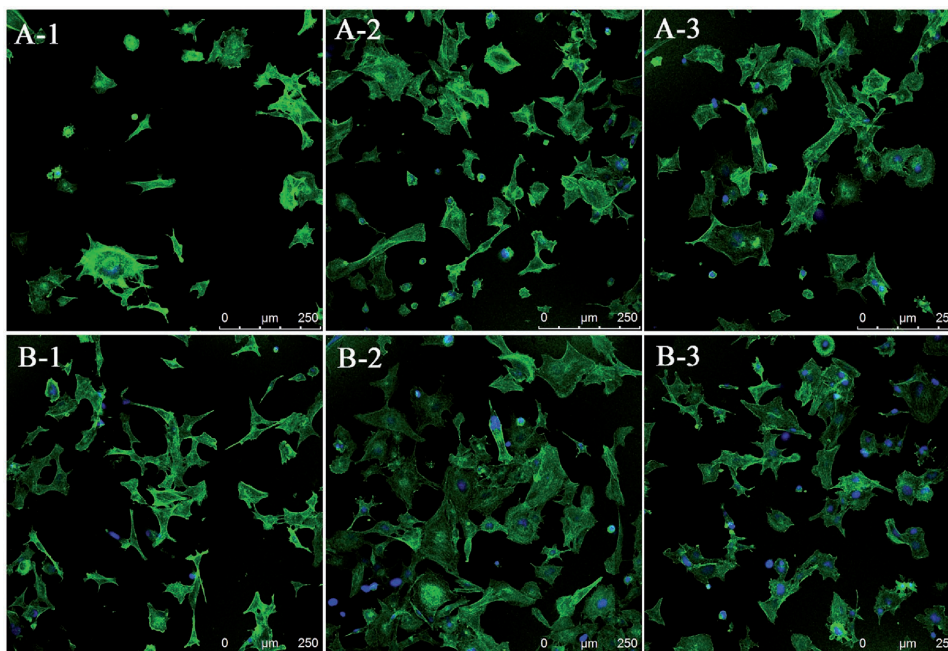


Figure 4. CLSM images of human osteoblast cells adhered on the samples A) without and B) with the preadsorption of Vn cultured in serum-free medium (1: the untreated sample, 2: the $-\text{COOH}$ -grafted sample, 3: the $-\text{NH}_2$ -grafted sample). The F-actin and nucleus are labeled in green and blue, respectively.

exhibit very well stretching state and are homogeneous with the actin being organized into stress fibers. The cells attached on the $-\text{COOH}$ -grafted surfaces exhibit more rounded phenotype, whereas the cells on the $-\text{NH}_2$ -functionalized surfaces show more spindled morphology. Methyl thiazole tetrazodium (MTT) assessment of the cells cultured in serum-free Dulbecco's modified eagle's medium (DMEM) suggests more adhered cells on the films with preadsorption of Vn than on the non-preadsorption films (Figure 5). This in turn indicates that adsorbed Vn

indeed promotes osteoblast adhesion. Strikingly, it is also noted that among all the samples, the $-\text{COOH}$ -grafted surface with preadsorption of Vn exhibits the most abundant adhered cells. $-\text{NH}_2$ -grafting also brings about significantly enhanced cell adhesion, even though the effect is slightly weaker than that exerted by the preadsorption of Vn.

It is clear that preadsorbed Vn facilitates cell adhesion and spreading, and this is in fact attributed to exposure of the cell binding domain of the protein.^[6a,23] Our results also show that upon adsorption on the $-\text{COOH}$ -grafted surfaces, Vn opted to form multimeric aggregates (Figure 2) with intensified exposure of cell-binding domains (Figure 3). It is therefore likely that it is not the functional groups, $-\text{COOH}$ or $-\text{NH}_2$ in this case, that crucially influence the cell adhesion. Instead, the conformations of Vn adsorbed on the substrata decide predominately the fate of the cells. In addition, the most significant increase of cell adhesion occurs on the untreated samples (Figure 5), which may be partly due to altered surface wettability.^[24] The wettability of the surfaces after Vn adsorption was examined and the water contact angle is $61.3^\circ \pm 2.1^\circ$ for the untreated surface, $24.1^\circ \pm 3.2^\circ$ for the $-\text{COOH}$ modified surface, and $38.9^\circ \pm 3.6^\circ$ for the $-\text{NH}_2$ modified surface. The untreated surface is the most hydrophobic among the three surfaces (Figure 1B). Further Vn adsorption slightly decreases the water contact angle of the films and hydrophilic surfaces usually facilitate cell attachment.^[15b] Nevertheless, cell behaviors on the substrata are affected by many factors, among which conformation of the adsorbed protein plays very important roles.

To further elucidate the influence of the preadsorption of Vn on the cellular behaviors, expression of a number of integrin subunits of the cells adhered on the samples was examined (Figure 6). It is realized that the expression levels of *ITGA5*,

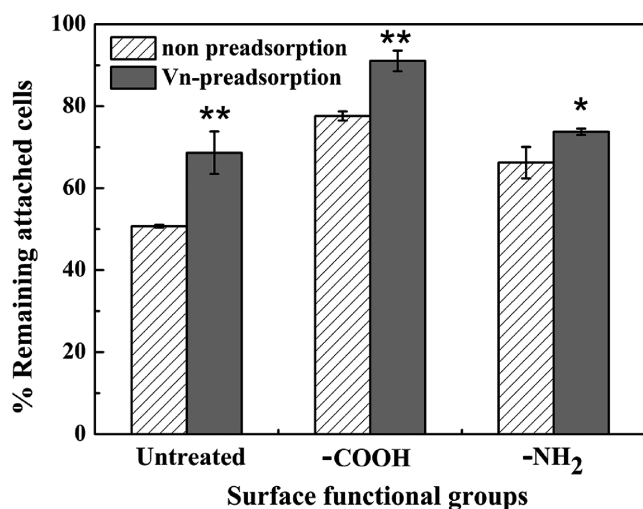


Figure 5. MTT assessment of the adhesion of the cells on the surfaces of the samples, the cells were cultured for 4 h in serum-free medium. Error bars refer to standard deviation ($n = 3$), * $p < 0.05$, ** $p < 0.01$ as compared with the control samples (analyzed by paired Student's *t*-test).

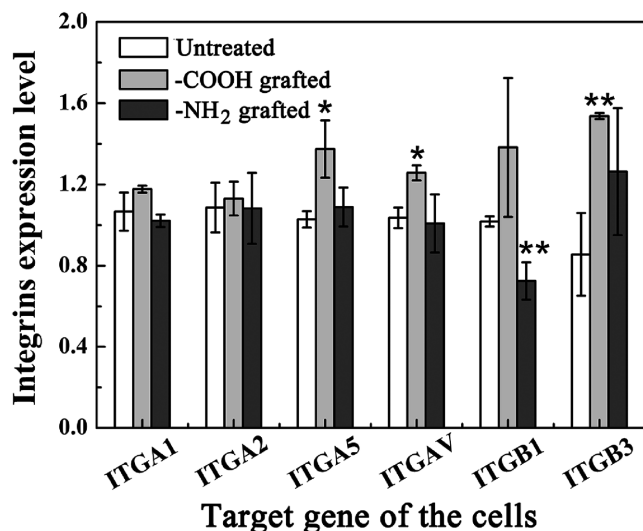


Figure 6. RT-PCR detection results showing the expression level of the selected integrin subunits of the cells adhered on the samples with alternative surface treatment. For the testing, the cells were plated on the samples with preadsorption of Vn for 4 h in serum-free medium. Error bars refer to standard deviation ($n = 3$), $*p < 0.05$, $**p < 0.01$ as compared with the control samples (analyzed by paired Student's *t*-test).

ITGAV, ITGB1, and ITGB3 are dramatically higher for the cells adhered on the -COOH-grafted surface than those adhered on the -NH₂-grafted surface. Other integrins show minor differences. It has been reported that Vn could specifically bind cell integrins, namely $\alpha_v\beta_1$, $\alpha_v\beta_3$, $\alpha_{2b}\beta_3$, and $\alpha_v\beta_5$, and these integrins recognize RGD motif to enhance cell adhesion, spreading, and differentiation.^[25] This is consistent with our results that higher expression of the integrins α_v , β_1 , and β_3 on the -COOH-grafted surfaces bears more exposed RGD sites of Vn for the more pronounced adhesion and spreading of the osteoblast cells. The integrin $\alpha_5\beta_1$ is a fibronectin receptor,^[26] and its high expression level possibly suggests that the adsorbed RGD-rich protein could stimulate the cells to produce RGD-rich extracellular matrix proteins, like fibronectin. These results further indicate that the conformational changes of the adsorbed Vn as regulated by the chemistry of substrata affect biological functions in gene levels of the cells.

3. Conclusion

Adsorption of Vn was examined by visualizing the molecule by negative-staining electron microscopy and its spatial alignment was analyzed by 2D image classification. Charging state of the substrata significantly affects the conformations of adsorbed Vn and the molecules tend to form multimer aggregates on -COOH-grafted surface, exposing extensively the cell-binding domain. On the -NH₂-treated surface, Vn opts to form dimer aggregates. Gene expression analyses of the osteoblast cells attached on the model surfaces suggest remarkable impact of the conformations of adsorbed Vn on the cellular behaviors. The attempt of visualizing adsorbed Vn and interpreting the molecule conformations after adsorption would give insights into future study on biomaterial-cell interactions at molecule level.

4. Experimental Section

Preparation of Carbon Film Substrata for Protein Adsorption: Carboxylic acid (-COOH) and amine (-NH₂) functionalized surfaces were prepared by plasma grafting acrylic acid and allylamine on carbon-coated silicon wafers, following previously well-established protocols.^[27] Prior to the grafting, silicon wafers of 10 × 10 mm in width and length were washed with ethanol in an ultrasound bath, followed by rinsing with distilled water. The wafers were further cleaned using glow discharge cleaning system (PELCO easiGlow 91000, USA). Amorphous graphitic carbon films were produced by evaporating carbon layers under high vacuum (Cressington 208C Turbo Carbon Coater, USA). The deposition was carried out at 4.3 V for 20 s. The plasma grafting was conducted using an anode layer ion beam source (ALIS). For the grafting, the carbon-coated samples were placed into the plasma chamber situated between the externally located electrodes. The chamber was evacuated to 2×10^{-3} Pa, then glow-discharge was initiated by introducing oxygen gas. Current of the ALIS source and working power were 0.37 A and 128 W, respectively. Immediately after the discharge treatment, the samples were exposed in allylamine and acrylic acid vapor for 15 min to generate amine and carboxyl groups, respectively.

Surface Analyses: Surface chemistry of the materials was detected by XPS (ESCALAB 250, Thermo, USA) using Al (mono) K α irradiation, and C1s, O1s, and N1s core level signals were acquired. Further elemental and functional quantification was made using the Casa software. Wettability of the treated samples was examined by measuring contact angle of deionized distilled water droplets spreading on their surfaces by using a video-based optical contact angle measurement instrument (Dataphysics OCA20, Germany). Volume of each distilled water droplet was 3 μ L and five measurements were taken for an average value for each sample.

EM Characterization and 2D Image Classification: Adsorption behaviors of Vn were assessed by negative-staining EM analyses. Vn molecules isolated from human plasma (Sigma V8379, USA) were diluted in Milli-Q water for the adsorption testing on the plasma grafted thin carbon films standing on 300-mesh copper grids (TED Pella Inc., USA). A 5 μ L drop of Vn solution was applied onto the thin film sample and stayed for 2 min to ensure adsorption of Vn. After removing the excess solution by blotting with filter paper, the sample grid was stained by using two 5 μ L drops of 2% (w/v) uranyl acetate solution. Excess stain was removed by blotting, and the grids were quickly dried by air flow. Images were recorded under low-dose conditions (10 e \AA^{-2}) on field emission transmission EM (FEI Tecnai 20, USA) operated at 200 kV. Micrographs were acquired with a Gatan Ultrascan 4 k × 4 k charge coupled device camera at a magnification of 71 000 \times , corresponding to a pixel size of 1.97 \AA at the sample level. Picking and image processing of individual particle images were made using the software package EMAN.^[28] Over 5000 particles for each sample were used for the final reference-free 2D classification and image analyses. Surface rendering and preliminary docking of atomic structure were performed in University of California-San Francisco (UCSF) Chimera.^[29]

Characterization of Cell-Binding Domains of Vn: An enzyme-linked immunosorbent assay (ELISA) was performed to estimate the conformational change of adsorbed Vn. Each sample was coated with 5 μ L Vn solution (20 μ g mL⁻¹ in water) for 2 min, and excess solution was then removed by filter paper. The samples were blocked in 1% w/v BSA (bovine serum albumin)/PBS (phosphate buffered saline) for 1 h at 37 °C in shaker. After 3 times washing with PBST (PBS+tween) (0.05 vol% of tween-20 in PBS) solution, they were brought in contact with primary antibody (Abcam, UK) solution for 1 h at 37 °C and were then washed with PBST. Afterward the samples were incubated with a secondary antibody conjugated with HRP (horseradish peroxidase, Sangon Biotech, China) for 2 h. Reaction of the samples with stable colorimetric substrata was examined by tetramethyl benzidine assay (Sangon Biotech, China) after the final washing. Optical density was read on a microplate reader (Spectra max 190, USA) operated using the wavelength of 450 nm. For each condition, three samples were used for an average value.

Cell Culture Testing: Human osteoblast cell line (hFOB 1.19 SV40 transfected osteoblasts, the Type Culture Collection of Chinese Academy of Sciences, Shanghai, China) was employed for the cell culturing on

the carbon coated silicon with/without the additional modification with the functional groups. Cells were routinely cultured in DMEM (Gibco) supplemented with 10% fetal bovine serum (FBS, Quanshijin) and 2% penicillin-streptomycin (Gibco) in a humidified atmosphere at 37 °C and 5% CO₂. The cells were harvested with trypsin/EDTA (ethylenediaminetetraacetic acid) that could be inactivated by addition of FBS. Trypsinized cells were washed twice with serum-free medium to remove any trace of serum proteins.

Cell adhesion was examined using the MTT assay. Briefly, cells (5 × 10⁴ cells per well) were seeded on the substrata with/without preadsorbed Vn and they were placed in standard 24-well tissue culture plates for 4 h at 37 °C in the atmosphere of 100% humidity and 5% CO₂. After washing with PBS for three times, 50 µL of MTT stock solution was added into every well for 4 h. Subsequently, MTT solution was removed and 500 µL of DMSO (dimethyl sulphoxide) was added. The plate was rotated for 15 min at 37 °C and was read on the microplate reader using 490 nm wavelength.

For immunofluorescence assay analyses, cells were seeded onto the surfaces with/without preadsorbed Vn. After incubation for 4 h, the cells were rinsed with PBS for 3 times, and fixed with 4% paraformaldehyde for 20 min. They were then blocked by 1% BSA for 1 h. Actin filaments were stained with FITC-conjugated phalloidin (Sigma) for 90 min. Nuclei of the cells were labeled with DAPI (4',6-diamidino-2-phenylindole, Sigma) for 30 min. As the final step, all the samples were washed with PBS for three times and examined immediately with confocal laser microscope (CLSM, Leica TCS SP5, Germany).

In addition, gene expression levels of the cells were also assessed. Briefly, after 4 h culturing on the Vn-preadsorbed samples, the cells were harvested, and their total RNA was extracted using the Trizol reagent (RNAiso Plus, TaKaRa, China). RNA concentration was measured using NanoDrop 2000 (ThermoFisher, USA) at 260 nm prior to reverse transcription. The first-strand cDNA was synthesized using PrimeScript RT reagent Kit with gDNA Eraser (TaKaRa, China) and used as RT-PCR templates. Real-time PCR (polymerase chain reaction) was performed on a quantitative real-time amplification system (LightCycler 480II, Roche Applied Science, Germany) using SYBR Primix Ex Taq II (TaKaRa) following the manufacturer's protocol. The PCR conditions were 95 °C for 30 s followed by 40 cycles of 95 °C for 5 s and 60 °C for 20 s. Relative gene expression was determined by normalized to the expression of *GAPDH* in the same sample. The used primers are listed in Table 2.

Supporting Information

Supporting Information is available from the Wiley Online Library or from the author.

Acknowledgements

This work was supported by National Science Foundation of China (grant # 31271017, 31500772, and 41476064), China Postdoctoral Science Foundation (grant # 2016T90554), and Key Research and Development Program of Zhejiang Province (grant # 2017C01003).

Conflict of Interest

The authors declare no conflict of interest.

Keywords

cellular behaviors, conformational changes, protein adsorption, single particle EM, vitronectin

Received: August 6, 2017
Revised: September 7, 2017
Published online:

Table 2. Sequences of the primers used for the RT-qPCR analyses.

Gene	Sequence	Size [bp]
<i>ITGA1</i>	F AATTGGCTCTAGTCACCATTTGTT R CAAATGAAGCTGCTGACTGGT	87
<i>ITGA2</i>	F TCGTGCACAGTTTTGAAGATG R TGGAACACTTCCTGTTGTACC	71
<i>ITGA5</i>	F CCCATTGAATTTGACAGCAA R TGCAAGGACTTGACTCCACA	92
<i>ITGAV</i>	F GTTGCTACTGGCTGTTTTGG R CTGCTCCCTTTCTGTTCTTC	91
<i>ITGB1</i>	F TGCCGGGTTTCACTTTGC R GTGACATTGTCCATCATTTGGTAAA	70
<i>ITGB3</i>	F AATGCCACCTGCCTCAAC R GCTCACCGTGTCTCCAATC	78
<i>GAPDH</i>	F GCTCTCCAGAATCATCC R TGCTTACCACCTTCTTG	188

- [1] S. Bauer, P. Schmuki, K. Von der mark, J. Park, *Prog. Mater. Sci.* **2013**, *58*, 261.
- [2] C. J. Wilson, R. E. Clegg, D. I. Leavesley, M. J. Pearcy, *Tissue Eng.* **2005**, *11*, 1.
- [3] a) K. T. Preissner, *Blut* **1989**, *59*, 419; b) K. T. Preissner, *Annu. Rev. Cell Biol.* **1991**, *7*, 275.
- [4] D. Seiffert, J. W. Smith, *J. Biol. Chem.* **1997**, *272*, 13705.
- [5] F. Banovac, S. S. Saavedra, G. A. Truskey, *J. Colloid Interface Sci.* **1994**, *165*, 31.
- [6] a) H. P. Felgueiras, M. D. Evans, V. Migonney, *Acta Biomater.* **2015**, *28*, 225; b) H. F. Chieh, F. C. Su, J. D. Liao, S. C. Lin, C. W. Chang, M. R. Shen, *Soft Matter* **2011**, *7*, 3808; c) J. H. Seo, K. Sakai, N. Yui, *Acta Biomater.* **2013**, *9*, 5493; d) Y. Y. Li, Y. Wei, J. W. Liao, Y. W. Hao, C. G. Ning, L. Jiang, S. T. Wang, *Adv. Mater. Interfaces* **2016**, *3*, 1600598; e) L. Shang, L. X. Yang, J. Seiter, G. Brenner-Weiss, D. Gerthsen, G. U. Nienhaus, *Adv. Mater. Interfaces* **2014**, *1*, 1300079.
- [7] W. G. Pitt, D. J. Fabriziushoman, D. F. Mosher, S. L. Cooper, *J. Colloid Interface Sci.* **1989**, *129*, 231.
- [8] a) Q. Wei, T. Becherer, S. Angioletti-Uberti, J. Dzubiella, C. Wischke, A. T. Neffe, A. Lendlein, M. Ballauff, R. Haag, *Angew. Chem.* **2014**, *126*, 8138; *Angew. Chem., Int. Ed.* **2014**, *53*, 8004; b) H. L. Zhang, K. Bremmell, S. Kumar, R. S. C. Smart, *J. Biomed. Mater. Res., Part A* **2004**, *68*, 479; c) P. J. Molino, Z. L. Yue, B. B. Zhang, A. Tibbens, X. Liu, R. M. I. Kapsa, M. J. Higgins, G. G. Wallace, *Adv. Mater. Interfaces* **2014**, *1*, 1300122.
- [9] G. W. Lynn, W. T. Heller, A. Mayasundari, K. H. Minor, C. B. Peterson, *Biochemistry* **2005**, *44*, 565.
- [10] G. Deng, G. Royle, S. Wang, K. Crain, D. J. Loskutoff, *J. Biol. Chem.* **1996**, *271*, 12716.
- [11] R. C. Cherny, M. A. Honan, P. Thiagarajan, *J. Biol. Chem.* **1993**, *268*, 9725.
- [12] G. Deng, S. A. Curriden, S. J. Wang, S. Rosenberg, D. J. Loskutoff, *J. Cell Biol.* **1996**, *134*, 1563.
- [13] A. Mayasundari, N. A. Whittemore, E. H. Serpersu, C. B. Peterson, *J. Biol. Chem.* **2004**, *279*, 29359.
- [14] O. D. Liang, M. Maccarana, J. I. Flock, M. Paulsson, K. T. Preissner, T. Wadstrom, *Biochim. Biophys. Acta* **1993**, *1225*, 57.
- [15] a) P. Zhuang, A. I. Chen, C. B. Peterson, *Biochim. Biophys. Acta* **1997**, *272*, 6858; b) S. Bhakdi, R. Kaflein, T. S. Halstensen, F. Hugo, K. T. Preissner, T. E. Mollnes, *Clin. Exp. Immunol.* **1988**, *74*, 459.
- [16] a) C. Oehr, M. Muller, B. Elkin, D. Hegemann, U. Vohrer, *Surf. Coat. Technol.* **1999**, *116*, 25; b) J. J. A. Barry, M. M. C. G. Silva,

- K. M. Shakesheff, S. M. Howdle, M. R. Alexander, *Adv. Funct. Mater.* **2005**, *15*, 1134.
- [17] a) C. C. Barrias, M. C. L. Martins, G. Almeida-Porada, M. A. Barbosa, P. L. Granja, *Biomaterials* **2009**, *30*, 307; b) Y. Arima, H. Iwata, *Acta Biomater.* **2015**, *26*, 72; c) N. Faucheux, R. Schweiss, K. Lutzow, C. Werner, T. Groth, *Biomaterials* **2004**, *25*, 2721.
- [18] M. T. Bernardis, S. Y. Jiang, *J. Biomed. Mater. Res., Part A* **2008**, *87*, 505.
- [19] L. Baugh, V. Vogel, *J. Biomed. Mater. Res., Part A* **2004**, *69*, 525.
- [20] J. Zhou, S. F. Chen, S. Y. Jiang, *Langmuir* **2003**, *19*, 3472.
- [21] A. Stockmann, S. Hess, P. Declerck, R. Timpl, K. T. Preissner, *J. Biol. Chem.* **1993**, *268*, 22874.
- [22] K. T. Preissner, G. Mullerberghaus, *J. Biol. Chem.* **1987**, *262*, 12247.
- [23] S. Heydarkhan-Hagvall, J. M. Gluck, C. Delman, M. Jung, N. Ehsani, S. Full, R. J. Shemin, *Biomaterials* **2012**, *33*, 2032.
- [24] Y. Arima, H. Iwata, *Biomaterials* **2007**, *28*, 3074.
- [25] a) S. A. Mousa, *Med. Res. Rev.* **2003**, *23*, 190; b) P. Ylipaasto, M. Eskelinen, K. Salmela, T. Hovi, M. Roivainen, *J. Gen. Virol.* **2010**, *91*, 155; c) B. Felding-Habermann, D. A. Cheresh, *Curr. Opin. Cell Biol.* **1993**, *5*, 864; d) L. Heyman, S. Kellouche, J. Fernandes, S. Dutoit, L. Poulain, F. Carreiras, *Tumor. Biol.* **2008**, *29*, 231; e) D. Park, C. W. Park, Y. J. Choi, J. J. Lin, D. H. Seo, H. S. Kim, S. Y. Lee, I. C. Kang, *Biomaterials* **2016**, *98*, 131.
- [26] M. Kreiner, C. R. Chillakuri, P. Pereira, M. Fairhead, Z. H. Li, H. J. Mardon, S. A. Holt, C. F. Van der Walle, *Soft Matter* **2009**, *5*, 3954.
- [27] a) H. J. Jung, K. D. Ahn, D. K. Han, D. J. Ahn, *Macromol. Res.* **2005**, *13*, 446; b) K. Park, H. J. Jung, J. J. Kim, D. K. Han, *J. Bioact. Compat. Polym.* **2010**, *25*, 27; c) R. Olivares-Navarrete, S. E. Rodil, S. L. Hyzy, G. R. Dunn, A. Almaguer-Flores, Z. Schwartz, B. D. Boyan, *Biomaterials* **2015**, *51*, 69.
- [28] S. J. Ludtke, P. R. Baldwin, W. Chiu, *J. Struct. Biol.* **1999**, *128*, 82.
- [29] E. F. Pettersen, T. D. Goddard, C. C. Huang, G. S. Couch, D. M. Greenblatt, E. C. Meng, T. E. Ferrin, *J. Comput. Chem.* **2004**, *25*, 1605.